AFRL-RB-WP-TR-2009-3201

RISK QUANTIFIED STRUCTURAL DESIGN AND EVALUATION

Eric J. Tuegel

Analytical Mechanics Branch
Structures Division

SEPTEMBER 2009

Final Report

AIR FORCE RESEARCH LABORATORY
AIR VEHICLES DIRECTORATE
WRIGHT-PATTERSON AIR FORCE BASE, OH 45433-7542
AIR FORCE MATERIEL COMMAND
UNITED STATES AIR FORCE

NOTICE AND SIGNATURE PAGE

Using Government drawings, specifications, or other data included in this document for any purpose other than Government procurement does not in any way obligate the U.S. Government. The fact that the Government formulated or supplied the drawings, specifications, or other data does not license the holder or any other person or corporation; or convey any rights or permission to manufacture, use, or sell any patented invention that may relate to them.

This report was cleared for public release by the Air Force Research Laboratory Air Vehicles Public Affairs Office and is available to the general public, including foreign nationals. Copies may be obtained from the Defense Technical Information Center (DTIC) (http://www.dtic.mil).

AFRL-RB-WP-TR-2009-3201 has been reviewed and is approved for publication in accordance with assigned distribution statement.

*//signature//_____
ERIC J. TUEGEL
Project Engineer
Analytical Mechanics Branch
Structures Division

//signature//_____
ANDREW G. SPARKS, Chief
Analytical Mechanics Branch
Structures Division

//signature//_____
DAVID PRATT, Technical Advisor
Structures Division
Air Vehicles Directorate

This report is published in the interest of scientific and technical information exchange, and its publication does not constitute the Government's approval or disapproval of its ideas or findings.

*Disseminated copies will show "//Signature//" stamped or typed above the signature blocks.

REPORT DOCUMENTATION PAGE

Form Approved
OMB No. 0704-0188

1. REPORT DATE *(DD-MM-YY)*	2. REPORT TYPE	3. DATES COVERED *(From - To)*
September 2009	Final	01 October 2004 – 30 June 2009

4. TITLE AND SUBTITLE
RISK QUANTIFIED STRUCTURAL DESIGN AND EVALUATION

5a. CONTRACT NUMBER
F33615-00-D-3052-0086

5b. GRANT NUMBER

5c. PROGRAM ELEMENT NUMBER
0602201

6. AUTHOR(S)
Eric J. Tuegel

5d. PROJECT NUMBER
A07X

5e. TASK NUMBER

5f. WORK UNIT NUMBER
0E

7. PERFORMING ORGANIZATION NAME(S) AND ADDRESS(ES)
Analytical Mechanics Branch (AFRL/RBSM)
Structures Division
Air Force Research Laboratory
Air Vehicles Directorate
Wright-Patterson Air Force Base, OH 45433-7542
Air Force Materiel Command
United States Air Force

8. PERFORMING ORGANIZATION REPORT NUMBER

9. SPONSORING/MONITORING AGENCY NAME(S) AND ADDRESS(ES)
Air Force Research Laboratory
Air Vehicles Directorate
Wright-Patterson Air Force Base, OH 45433-7542
Air Force Materiel Command
United States Air Force

10. SPONSORING/MONITORING AGENCY ACRONYM(S)
AFRL/RBSM

11. SPONSORING/MONITORING AGENCY REPORT NUMBER(S)
AFRL-RB-WP-TR-2009-3201

12. DISTRIBUTION/AVAILABILITY STATEMENT
Approved for public release; distribution unlimited.

13. SUPPLEMENTARY NOTES
PAO Case Number: 88ABW 2009-3861, 03 September 2009. Report contains color.

14. ABSTRACT
The objective of this program was to investigate the risk-quantified design methods for the design and certification of the structure for future military aircraft. The current Department of Defense (DoD) process for developing and supporting aircraft structures relies heavily on testing, including full-scale testing, to ensure structural integrity and reliability. This process adds cost and time to any new development program or service life extension effort. In the future DoD vision of lean, agile acquisition programs, a new paradigm is needed for making decisions about the airworthiness of an aircraft. Other industries, such as nuclear power and offshore oil, have developed a risk quantification process for deciding if a given structure should be placed in service. A similar risk quantification process could be applied in the airworthiness decision process for small aircraft fleets and hypersonic aircraft after adapting it to the DoD procurement process, the aircraft design process, and the safety issues particular to aircraft.

15. SUBJECT TERMS
risk, probabilistic design, probability of failure

16. SECURITY CLASSIFICATION OF:			17. LIMITATION OF ABSTRACT:	18. NUMBER OF PAGES	19a. NAME OF RESPONSIBLE PERSON (Monitor)
a. REPORT	b. ABSTRACT	c. THIS PAGE			Eric J. Tuegel
Unclassified	Unclassified	Unclassified	SAR	36	19b. TELEPHONE NUMBER *(Include Area Code)* N/A

Standard Form 298 (Rev. 8-98)
Prescribed by ANSI Std. Z39-18

ABSTRACT

The objective of this program was to investigate the risk-quantified design methods for the design and certification of the structure for future military aircraft. The current Department of Defense (DoD) process for developing and supporting aircraft structures relies heavily on testing, including full-scale testing, to ensure structural integrity and reliability. This process adds cost and time to any new development program or service life extension effort. In the future DoD vision of lean, agile acquisition programs, a new paradigm is needed for making decisions about the airworthiness of an aircraft. Other industries, such as nuclear power and offshore oil, have developed a risk quantification process for deciding if a given structure should be placed in service. A similar risk quantification process could be applied in the airworthiness decision process for small aircraft fleets and hypersonic aircraft after adapting it to the DoD procurement process, the aircraft design process, and the safety issues particular to aircraft.

The Risk Quantified Structural Design and Evaluation – Warm Primary Structure (RQSD&E) program was conducted in two phases. The first phase was exploratory determining the advantages of risk quantified structural evaluations of simple structural configurations. The second phase focused on developing simple techniques to accomplish the following three things:

1) Identify structural items that affect vehicle reliability or safety (important structural items),
2) Design structural components for a specified probability of failure, and
3) Validate structural models with a limited number of data containing variability, or uncertainty.

This project determined that the challenge for risk-quantified design and evaluation does not seem to be in developing new more sophisticated probabilistic techniques, but in getting the existing techniques into common practice. It needs to become relatively easy for the average engineer without a lot of expertise in probabilistic technology to use probabilistic methods. The way to do this is to make incremental changes to existing design and maintenance processes by enabling engineers to readily obtain more and better information upon which to base any decisions about the airworthiness of an aircraft upon.

Table of Contents

List of Figures

List of Tables

1.0 INTRODUCTION

The objective of this program was to investigate the risk-quantified design methods for the design and certification of the structure for future military aircraft. The current Department of Defense (DoD) process for developing and supporting aircraft structures relies heavily on testing, including full-scale testing, to ensure structural integrity and reliability. This process adds cost and time to any new development program or service life extension effort. This has been acceptable because the cost of half a dozen test aircraft and the associated testing cost and time is insignificant compared to the several hundred aircraft being bought. Compared to the production schedule for these large numbers of aircrafts the several years of testing time was acceptable. However, the future vision for DoD aircraft purchases is lean, agile programs that efficiently produce less than ten aircraft of a given type. In this situation, the addition of a single airframe for testing can increase the program cost by 10% or more. And the years required to complete the tests could be longer than the production schedule. Therefore, another process is needed to ensure aircraft structural integrity in these lean, agile acquisition programs.

Other industries, such as nuclear power and offshore oil, offer alternatives to the current build-and-test paradigm. In both industries, structural integrity is an important attribute. Because of the uniqueness of each structure or its operating conditions, testing is not a viable approach for evaluating structural integrity. Both industries have developed a risk quantification process for deciding if a given structure should be placed in service. A similar risk quantification process could be applied in the airworthiness decision process for small aircraft fleets and hypersonic aircraft after adapting it to the DoD procurement process, the aircraft design process, and the safety issues particular to aircraft. The risk quantification process must work within the Systems Engineering Process.

2.0 METHODS, ASSUMPTIONS, AND PROCEDURES

The Risk Quantified Structural Design and Evaluation – Warm Primary Structure (RQSD&E) program was conducted in two phases. The first phase was exploratory determining the advantages of risk quantified structural evaluations of simple structural configurations. The second phase focused on developing simple techniques to accomplish the following three things:

1) Identify structural items that affect vehicle reliability or safety (important structural items),
2) Design structural components for a specified probability of failure, and
3) Validate structural models with a limited number of data containing variability, or uncertainty.

2.1 Exploration

The objective of this phase was to demonstrate the benefits of probabilistic design and risk assessment for aircraft structural design. Two benchmark problems were selected to demonstrate the benefits: the thermal buckling response of a rectangular panel [1], and the thermal buckling response of the wing skin of a conceptual hypersonic aircraft [2]. In addition to using these benchmark problems to investigate the benefits of probabilistic design and risk assessments, practical methods for reliability-based design of aerospace structures were investigated.

The exploratory investigations and their detailed results were reported in two reports [1, 2]. These investigations concluded that probabilistic analysis provides a way to determine how variability in loading, geometry, materials, and environment affect the reliability of a design and the contribution of each design parameter. Probabilistic design requires a number of analyses, typically finite element analyses for structures. General purpose probabilistic analysis software packages, such as NESSUS® [3] and UNIPASS™ [4], that can automatically control the analysis process are commercially available. These codes also provide information on the sensitivity of the results to various input parameters. This sensitivity information is useful in driving towards more robust designs.

There are several major issues which deter the use of probabilistic design practices. These issues include:

- defining reliability design criteria for the system and the individual components;
- handling geometric variability that requires new finite element models and meshes; and
- determining the probability distributions for design parameters with limited information.

2.2 Technique Development

The techniques developed during the second phase of this program have been reported in several journal papers and conference presentations. Only those techniques not presented elsewhere are presented in detail. References are provided to papers and presentations discussing the remaining techniques.

2.2.1 Identifying Important Structural Items

Important Structural Items are defined as structural details that either contribute greatly to the reliability of the airframe, Reliability Critical Structural Items (RCSIs), or significantly impact the structural integrity and safety of the airframe, Significant Structural Items (SSIs). As depicted in Figure 1, these two sets of structural details comprise two subsets of the entire airframe. RCSIs are the locations and components with a higher probability of failure and significantly affect the overall system reliability. SSIs may or may not have a high probability of failure; however, if an SSI fails the aircraft will be lost. Hence, some details may be contained in both subsets, but it is not necessary for the two subsets to be coincident.

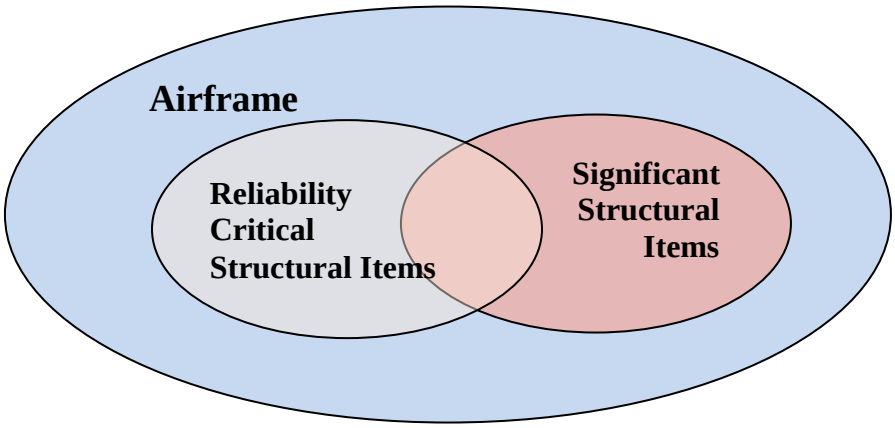

Figure 1: Depiction of Relation between Reliability Critical Structural Items and Significant Structural Items

The goal of this effort was to develop well-defined processes for identifying these two types of structures using the structural models to supplement experience and engineering judgment as to what structural components are important. Structural components identified as important can then be treated with special attention during design, fabrication, assembly and maintenance. For instance, important structural components can be subjected to special analysis checks during design, special inspections during fabrication and assembly, and identified as locations for health monitoring sensors in service.

2.2.1.1 Identifying Reliability Critical Structural Items

A technique for rapidly screening structural failure modes and locations to determine those that contribute most to the reliability of the airframe was developed. The method uses a formal error metric to quantify the error incurred with respect to the system reliability if a particular location is filtered, i.e., removed from the set of locations whose probability of failures are considered to contribute to the system probability of failure. Locations with errors below a user-defined probability of failure threshold (typically in the range of 10^{-4} to 10^{-8}) are filtered; these locations contribute little to the overall system reliability. The method integrates naturally with a first-order reliability method (FORM) representation of the failure modes and is very fast (one million limit states can be filtered in 2 hours on a desktop machine). A hierarchical multi-level approach

has been developed to verify the important limit states. The procedure for performing this screening has been demonstrated for an aircraft wing [5-6], an exhaust manifold for an internal combustion engine [6], and has been verified using Monte Carlo sampling. Further validation efforts will include comparison against tests of a T-38 longeron.

2.2.1.2 Identifying Significant Structural Items

A method for identifying SSIs using vulnerability analysis was investigated. A structure, or any part of it, is vulnerable when relatively small damage to the structure leads to disproportionately large consequences, such as inability to carry limit load or the structure becoming a mechanism [7]. Preliminary results in Penmetsa, et al. [8] indicated potential to identify structural elements, or regions, that are vulnerable even when they are not highly loaded or have a low probability of failure.

The challenge is that numerous analyses of the structure are required considering failure at each structural location in turn. A technique for performing these analyses without having to recompile the global stiffness matrix in a finite element model was developed to make these analyses less cumbersome. The technique utilizes the fact that a failure in a single location does not dramatically change the global stiffness matrix.

2.2.2 Designing to a Specified Probability of Failure

Most aerospace engineers intuitively understand that using a larger factor of safety (uncertainty) and/or margin of safety will result in a more reliable part. However, the actual reliability of the part has never quantified to determine how much larger or lower these factors need to be. Simple relationships between the factor of safety (uncertainty), or the margin of safety, and the probability of failure from static overstress were developed for general distributions of load and strength in [9-10]. Similarly, a method for computing the probability of fracture for a cracked structure subjected to a defined loading distribution using a three chart nomograph was developed [11-13].

While developing these methods, it became apparent that there was a need to find the distribution for the product or ratio of random variables. There were no general methods for making these calculations, so a procedure was developed.

2.2.2.1 Finding Products and Quotients of Distributions

Ravi Penmetsa
Wright State University

Determining the distribution of the product, or ratio, of random variables is a common operation in structural reliability analyses. The strength distribution and the cross section area distribution must be multiplied together to determine the distribution for the failure load of a structural element so that the probability that the applied loads exceed the failure load can be computed. Or the applied load distribution needs to be divided by the cross sectional area distribution to obtain the distribution of applied stress.

Most efforts towards developing methods for determining the distribution for the product, or ratio, of random variables have concentrated on methods that produce closed-form, analytical Probability Distribution Functions (PDF) for products of variables with particular types of distributions [14-21]. Recently, methods capable of handling mixed families of distributions like a product of Gamma and Weibull distributions have been developed [22]. While these methods are limited to obtaining a PDF for the product of two random variables, Podolski [23] has presented a technique to determine the PDF of a product of "n" variables. However, this method is restricted to Gamma distributions.

There are no methods for situations where the variables are from arbitrary families of distributions. Many times the distributions for the random variables in structural reliability analysis are different from those distributions for which the closed form solutions are available. Moreover, it is impractical to implement a general structural reliability analysis routine where different solution approaches are required for different factor distributions.

The method described here is applicable to the product or ratio of any number of random variables and has no restriction on the type of PDFs. One of the drawbacks of this methodology is that it is restricted to only non-negative random variables. However, in structural applications random variables representing geometric parameters and material strength variations are always positive. Several examples are presented to demonstrate the proposed method.

2.2.2.1.1 Product and Ratio of Random Variables

Let $Y=X_1X_2$ be the product of two random variables whose PDFs are defined by f_1 and f_2. The PDF of $Y(f_Y)$ is obtained as follows:

1. Take the logarithm of both sides of $Y=X_1X_2$:

$$\log [Y] = \log [X_1X_2] = \log [X_1] + \log [X_2] \quad (1)$$

2. Recast the equation in terms of new variables Z, A_1, and A_2:

$$Z = \log [Y] = \log [X_1] + \log [X_2] = A_1 + A_2 \quad (2)$$

3. Determine the PDFs of A_1 and A_2 using the chain rule for PDF transformation. This will be discussed in the following section.
4. Determine the PDF of the sum, $Z = A_1 + A_2$, using the convolution integral. This is a straightforward approach for standard distributions like normal, Weibull, etc. Since A_1 and A_2 may not have standard PDFs, the PDF of the sum is evaluated using Fast Fourier Transformation (FFT) based convolution. Details of the FFT convolution process are presented in the section titled "Convolution Using Fast Fourier Transform".
5. Transform the PDF of Z using the chain rule to determine the PDF of Y = exp[Z].

These steps are applicable to both the product and the ratio of any number of independent random variables with any random distributions. The final PDF obtained using this approach will

be a discrete set of data points representing the PDF values for the range of Y. While this approach does not directly produce closed form equations for the final PDF, a general method for fitting a weighted sum of beta distributions can be used to determine a closed form equation for the final distribution if needed. Many structural reliability analysis tools handle discrete PDF definitions without the need for actual closed form equations [24].

2.2.2.1.2 Transformation of Random Variables

The expression for the PDF, $f_A(A)$, of a variable $A=g(x)$ can be determined by differentiating its Cumulative Distribution Function (CDF), $F_A(A)$. [25]

$$f_A(A) = \frac{d}{dA} F_A(A) = \frac{d}{dA} F_x\left(g^{-1}(A)\right) = \frac{d}{dA}\left[\int_{-\infty}^{g^{-1}(A)} f_x(x)dx\right] \tag{3}$$

This can be further simplified to

$$f_A(A) = \frac{dg^{-1}(A)}{dA} f_x\left(g^{-1}(A)\right) = \frac{dx}{dA} f_x(x) \tag{4}$$

Using this chain rule, the PDF for $A = log(x)$ is found to be

$$\begin{aligned} &A = \log(x) \\ &\frac{dx}{dA} = e^A = x \\ &f_A(A) = \frac{dx}{dA} f_x(x) = x f_x(x) = e^A f_x\left(e^A\right). \end{aligned} \tag{5}$$

Equations (5) derive the PDF of $log(x)$ given the PDF of the variable x. The inverse operation of determining the PDF for $A = exp(x)$ is

$$\begin{aligned} &A = \exp(x) \\ &\frac{dx}{dA} = \frac{1}{A} = \frac{1}{e^x} \\ &f_A(A) = \frac{dx}{dA} f_x(x) = \frac{1}{e^x} f_x(x) = \frac{1}{A} f_x(\log(A)). \end{aligned} \tag{6}$$

The last transformation will be done on a pointwise representation of the PDF, $f_x(x)$.

2.2.2.1.3 Convolution Using Fast Fourier Transformation

Fast Fourier Transform (FFT) based convolution is a well-developed technique and has been

used for many decades in signal processing. The FFT algorithm derives its efficiency by transforming the physical domain into the frequency domain. Convolution in the physical domain is converted to an algebraic product of two signals (PDFs in this case) in the frequency domain. The FFT-based convolution algorithm for a generic problem of the form X-aY is outlined below.

Step 1: FFT-based convolution is applicable for the sum of random variables. Therefore, X-aY needs to be put in the form $X+Z$. This can be done by introducing a variable $Z = -aY$. The PDF of Z can be determined using chain rule as follows

$$f_Z = \frac{dY}{dZ} f_Y = \left|\frac{-1}{a}\right| f_Y\left(\frac{-z}{a}\right) \tag{7}$$

Step 2: Once the function is expressed as a sum of two random variables X and Z, their PDF's need to be discretized using a common discretization. This discretization enables implementation of an efficient Discrete FFT algorithm. The discretization of the PDF's is determined based on the number of points and the bounds of the variables used for the convolution. Most FFT algorithms are optimized to handle points as powers of 2. Therefore, 2^{10} (=1024) to 2^{12} (=4096) points will be used in this paper. A convergence study can be performed to determine the number of points required to give the desired accuracy. Once the number of points is defined, the smallest range (UpperLimit - LowerLimit) of X and Z is selected to determine the discretization increment. The smallest range is used so that both the distributions will be at least the selected number of points.

This discretization step yields two vectors with different numbers of elements depending on the range of X and Z. For example, consider a case where X is a random variable with range [0, 4] representing the entire area under its PDF, and Z has a range [3, 9]. If the required number of points was determined to be 2^{10}, then the discretization increment would be

$$\Delta = \frac{4-0}{2^{10}} = 0.0039. \tag{8}$$

When the PDF of Z is discretized using the same increment, the size of the vector for Z would be

$$S_Z = \frac{9-3}{\Delta} = 1539 = 2^{10} + 515 \approx 2^{10} + 2^9. \tag{9}$$

However, in order to apply discrete FFT algorithm the sizes of the vectors need to be equal. Therefore, 2^9 zero-valued elements are added to the upper end of the X-vector extending its range from [0,4] to [0,6].

With this operation both the vectors have equal numbers of elements but the number of elements in the vectors is not a power of 2. Two final operations are performed that add additional zeros until the size of each vector is equal to a power of 2, and then double the size of the vectors. The

first operation, making the size a power of 2, ensures better efficiency since the discrete FFT algorithms are optimized to deal with powers of 2. The second operation, doubling the size of the vector, eliminates the circular convolution issue of discrete FFT. Both operations increase the range of the vectors.

For the above example, the vectors $X[0, 6]$ and $Z[3, 9]$ are of size $2^{10}+2^{9}$. Since the next power of 2 is 2^{11}, 2^{9} zero-valued elements are added to both vectors. The new ranges of the two vectors are $X[0, 8]$, and $Z[3, 11]$.

Step 3: Once the discrete vectors have been constructed, the next step is to obtain the FFT of each of these vectors. FFT routines are standard functions in many mathematical software packages and spreadsheets.

Step 4: The FFT converts the convolution of two PDF's, *X* and *Z*, into the product of two vectors, *A* and *B*. Both these vectors are multiplied element by element using complex number multiplication for the entire length of the vector *A* to obtain the resultant vector, *C*.

Step 5: The inverse FFT of the vector *C* will yield the PDF of the initial function represented by $X - aY$.

Step 6: The range of the final PDF, $X-aY$, is determined from the ranges of *X* and *Z*. Since the final distribution is the sum of the two variables, *X* and *Z*, the range of $X-aY$ is the interval found by adding the two ranges. Based on the values selected earlier, for $X[0, 8]$ and $Z[3, 11]$, then the range for $X-aY$ is $[0+3, 8+11] = [3, 19]$. It should be noted that the size of the final vector is equal to the size of the input vectors after doubling their length.

FFT-based convolution is highly efficient once implemented and can be applied to problems with any PDF distributions without the need for any approximations of the PDF. Therefore, FFT-based convolution is ideal for implementing as a general convolution routine.

2.2.2.1.4 Numerical Examples

The following examples are selected to demonstrate the FFT-based joint PDF modeling process for the product and ratio of random variables. The first example is selected to demonstrate the accuracy of the presented numerical technique compared to analytical solutions. The second example demonstrates product of four random variables. And the third example demonstrates the combination of product and ratio of variables.

Example 1:
In this example, the PDF of a random variable, $Z=XY$, is determined using the FFT-based convolution technique. Glen, et al., [26] have developed an analytical solution for the situation where X ~ Uniform[1,2] and Y~Uniform[3,4]. These same uniform distributions are considered here to compare the numerical solution to the analytical solution. The analytical solution is:

$$\text{PDF of Z} = f_Z = \begin{cases} Log[z] - Log[3], & 3 < z < 4 \\ Log[4] - Log[3], & 4 < z < 6 \\ 3Log[2] - Log[z], & 6 < z < 8 \end{cases} \qquad (11)$$

Following the steps outlined in the previous section, the PDF of *Z* is determined from the FFT-based convolution of *log[X]* and *log[Y]*. For this example, 2^{10} points were used to discretize the PDFs of the two random variables; Δ is equal to 0.00098. The intermediate distributions used to find the PDF of *Z* are:

$$A = \log(X), \quad B = \log(Y)$$
$$f_A(A) = e^A \quad \text{for} \quad A \in [0, \log(2)]$$
$$f_B(B) = e^B \quad \text{for} \quad B \in [\log(3), \log(4)]$$

Figure 2 shows the agreement between the numerical solution and the analytical solution.

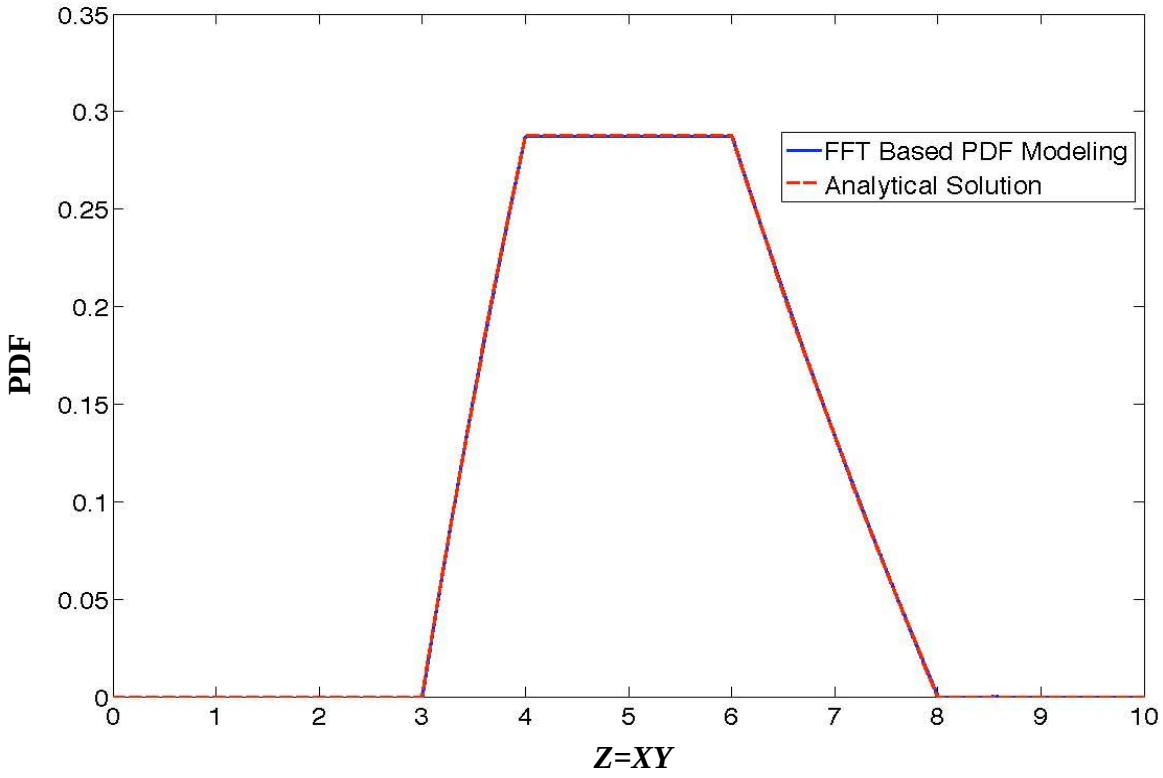

Figure 2: Comparison of Analytical and Numerical Solutions for PDF of Z=XY

Example 2:

In this example, product of four random variables is considered $Z=X_1X_2X_3X_4$. The PDF of log[Z] is merely the convolution of the PDFs of log[X_1], log[X_2], log[X_3], and log[X_4]:

$$\log Z = \log X_1 + \log X_2 + \log X_3 + \log X_4 \tag{12}$$

The distributions were selected as follows X_1~Normal[100,10], X_2~Weibull[100, 3.5], X_3~Rayleigh[25], X_4~Uniform[75, 100] to demonstrate the applicability of the method to any combination of distributions. Since an analytical solution in not available for this situation, Monte Carlo simulation was used to estimate the PDF of the product.

The distributions used in the convolution are:

$$A = \log X_1, \quad B = \log X_2, \quad C = \log X_3, \quad D = \log X_4,$$

$$f_A(A) = \frac{1}{10\sqrt{2\pi}} \exp\left[A - \frac{1}{2}\left(\frac{e^A - 100}{10} \right)^2 \right],$$

$$f_B(B) = \frac{3.5}{100^{3.5}} \exp\left[3.5B - \left(\frac{e^B}{100} \right)^{3.5} \right], \tag{13}$$

$$f_C(C) = \frac{1}{25^2} \exp\left[2C - \frac{1}{2}\left(\frac{e^C}{25} \right)^2 \right],$$

$$f_D(D) = \frac{e^D}{25}.$$

It can be seen in Figure 3 that FFT-based approach for determining the PDF of the product of four arbitrary distributions matches the PDF resulting from the Monte Carlo simulations.

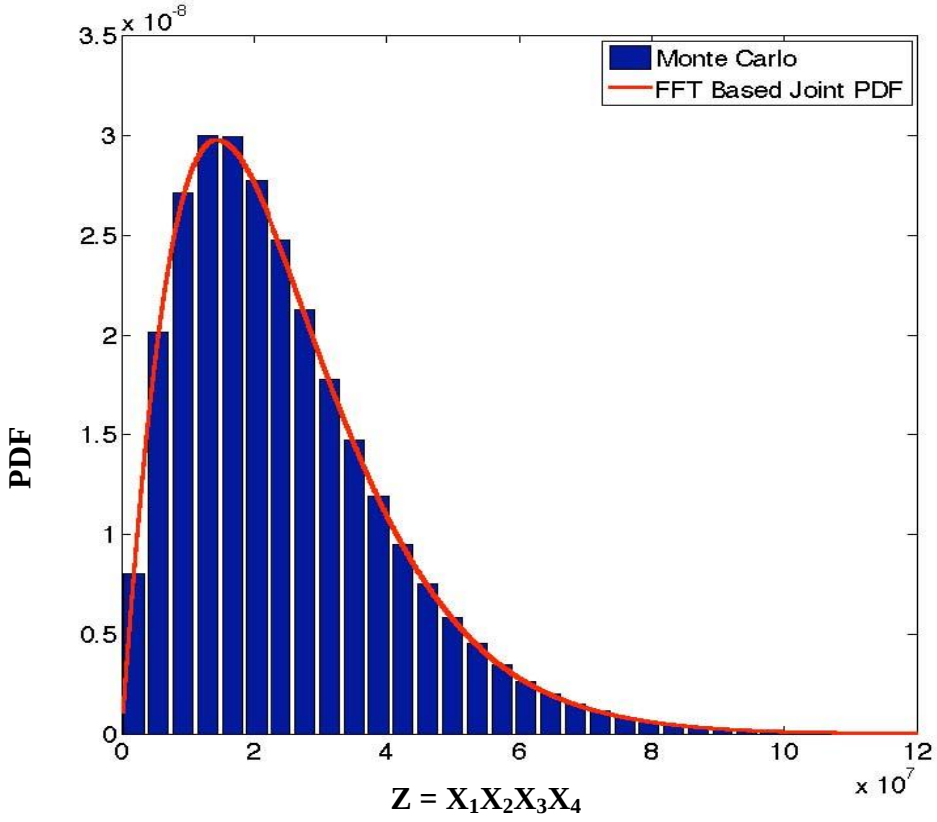

Figure 3: PDF of Product of Four Variables

Example 3:
In this example, a combination of both product and ratios of random variables is considered:

$$Z = \frac{X_1 X_2}{X_3 X_4^{2.5}}, \qquad (14)$$
$$\log Z = \log X_1 + \log X_2 - \log X_3 - 2.5 \log X_4 .$$

Monte Carlo simulation is once again used to estimate the PDF of Z in order to verify the FFT-based approach. The following distributions were used in this example: X_1~Weibull[1000, 3.5], X_2~Rayleigh[25], X_3~Normal[500, 80], X_4~Uniform[25, 50]. The intermediate distributions needed for the convolution are:

$$A = \log X_1, \quad B = \log X_2, \quad C = \log X_3, \quad D = \log X_4,$$

$$f_A(A) = \frac{3.5}{1000^{3.5}} \exp\left[3.5A - \left(\frac{e^A}{1000} \right)^{3.5} \right],$$

$$f_B(B) = \frac{1}{25^2} \exp\left[2B - \frac{1}{2}\left(\frac{e^B}{25} \right)^2 \right], \tag{15}$$

$$f_C(C) = \frac{1}{10\sqrt{2\pi}} \exp\left[C - \frac{1}{2}\left(\frac{e^C - 100}{10} \right)^2 \right],$$

$$f_D(D) = \frac{e^D}{25}.$$

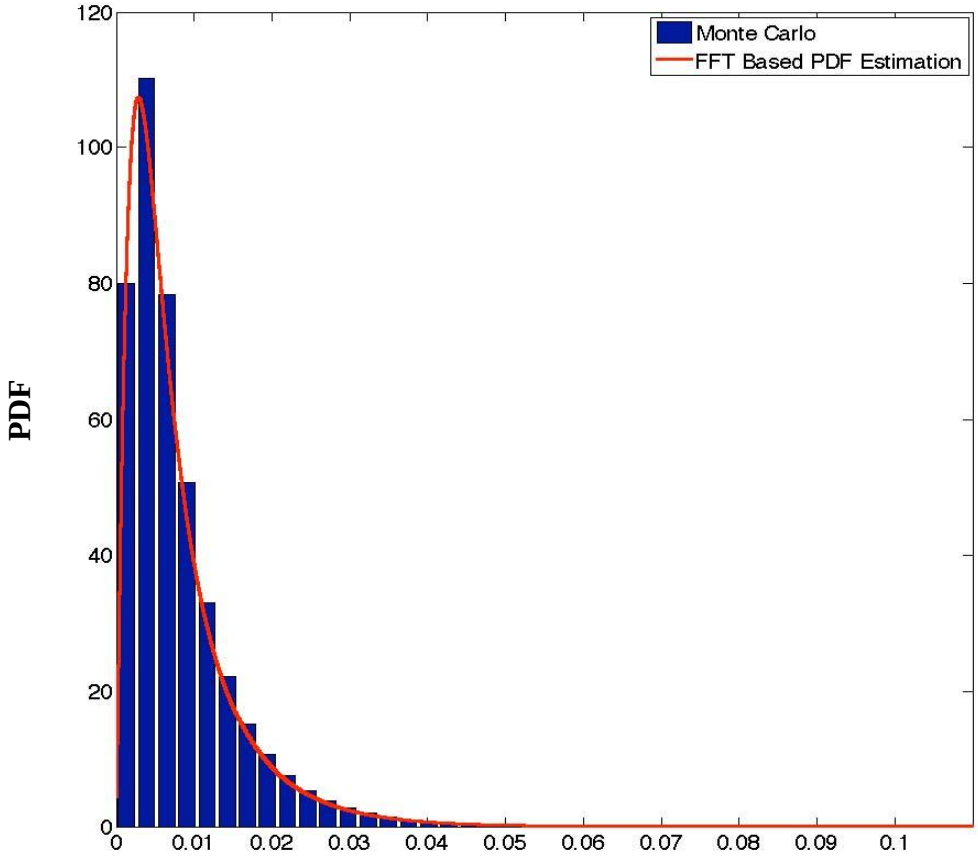

$$Z = \frac{X_1 X_2}{X_3 X_4^{2.5}}$$

Figure 4: PDF of a Combination of Product and Ratio of Random Variables

Figure 4 shows that the two results match accurately over the entire range of *Z*.

2.2.2.1.5 Summary of Finding Products and Quotients of Distributions

An FFT-based convolution method for determining the PDF of the product and ratio of random variables was found to be applicable to any distribution of random variables. This approach is applicable only to non-negative random variables. In most structural applications, the random variables are positive structural dimensions or material properties thereby making this approach useful for structural reliability analysis. This approach can be used along with regression models that have interaction terms that are products of random variables. Therefore, there are numerous applications for which this method can be used.

2.2.3 Quantifying Uncertainties in Large-Scale Numerical Simulations as Input to a Validation Framework

Jason Gruenwald, Daniel Nevill and Mark Brandyberry
University of Illinois, Urbana-Champaign

2.2.3.1 Introduction

A major obstacle to the use of large scale multi-physics simulations in design is proving that the simulations are reliable and valid. A methodology is needed to account for the uncertain inputs to the computational models, which cause difficulty in comparing results between the computational models and any available experimental data on the physical system being modeled. In order to capture the variability, probability distributions are used so that statistical measures of confidence can be used on the models to ensure they are reliable. Then, these simulations can be used to predict the responses from extreme conditions that would be nearly impossible to reproduce in a lab setting. However, it is often not feasible to directly produce uncertainty estimates for large computational models, since the simulations are potentially long-running and computationally intensive. This project was focused on developing a method for estimating this uncertainty with a minimum of computational effort.

The goal was to develop a large scale, multi-physics methodology that quantifies these uncertainties while minimizing the amount of computer simulation time. The end result is a probability distribution describing the likelihood of a set of response variables having certain values (described by probability distributions), which could play an integral part in design testing. This project investigated the use of a clustering methodology to produce the uncertainty quantification. The simulated system contained uncertainty in both fluid and structural elements, and thus the Computational Fluid Dynamics (CFD) modules from a simulation suite known as *Rocstar* was coupled with the finite element solver *Abaqus* to model the various aspects of the problem.

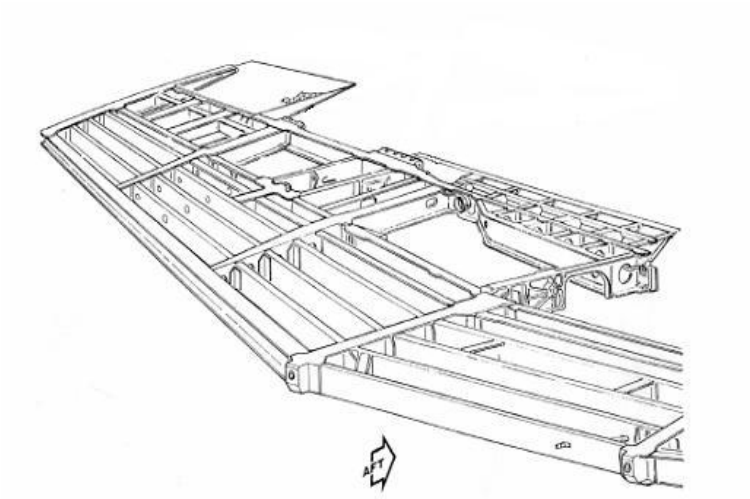

Figure 5: The internal structure of the wing

2.2.3.2 Description of Problem

The wing of a supersonic trainer aircraft was chosen for demonstration of the process. The wing has a sweep of 31.9° and a taper ratio of 0.2. It has a constant NACA 65A004.8 airfoil from the root to tip. For the simulations, only the aerodynamic and structural effects of the wing at 0° flaps were considered. The aerodynamic effects of the fuselage were ignored. The internal structure is shown in Figure 4.

2.2.3.3 Multi-Physics Models

2.2.3.3.1 Fluid Dynamics

To capture the uncertainty in the fluid portion of the simulation, a detailed, three-dimensional CFD package was used to model the air flow around the wing. The *Rocstar* suite is fully integrated to enable three-dimensional, multi-physics simulations. *Rocstar* is comprised of two CFD solvers, *Rocflo* and *Rocflu*. *Rocflo* is an explicit block-structured hexahedral solver, and *Rocflu* is an implicit unstructured mixed-mesh solver. For our purposes of determining the lift generated on the wing only the structured block fluids solver, *Rocflo*, was used.

In order to run a CFD analysis of the airflow about the wing of the aircraft, a mesh was created around the area of interest. This mesh is made of elements, and the governing equations of flow will be applied at each element. The mesh created for our purposes is fairly coarse, in order to limit the total computation time for this test problem. A finer mesh would produce a more accurate simulation of the flow, but would also increase the computation time. The mesh used in this simulation was comprised of approximately 600,000 elements. Due to symmetry only one half of the airplane was modeled, and it was assumed that the other half is symmetric in response. The grid was non-uniform, body-fitted, and the elements were smallest near the wing and increased in size further away. This gave the most accurate results at the elements nearest the wing, where we were most interested in the flow characteristics.

2.2.3.3.2 Solid Mechanics

A full scale idealized model of the wing, shown in Figure 6, was provided from the United States Air Force. The model was originally created in NASTRAN, but was translated into *Abaqus* for our simulations. It consisted of the wing and the main spars that attach the wing to the fuselage. It modeled the structurally relevant components, but did not model the leading edge or the control surfaces on the wing. The internal structure was idealized by beam, truss, shell and membrane elements. The wing was modeled with cantilever boundary conditions with extra pinned boundary conditions along the wing root to simulate the wing attachment to the fuselage. The loads were generated through CFD simulation as introduced in section 2.2.3.3.1, and were applied as pressure loads through an external transfer algorithm.

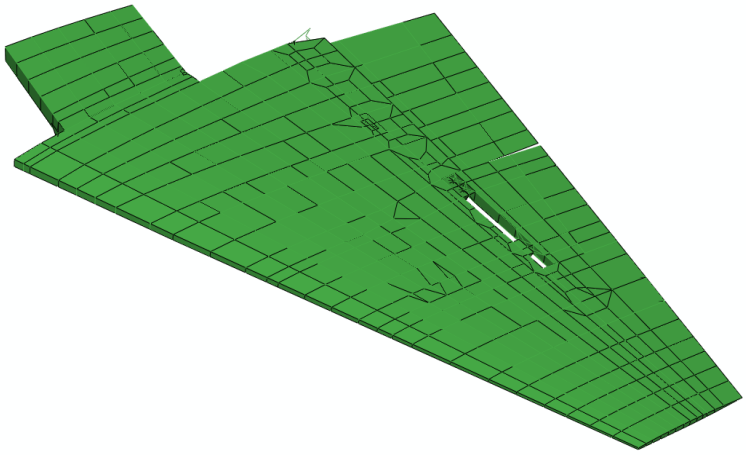

Figure 6: The idealized model of the wing was used in Abaqus for the full scale simulations

2.2.3.4 Uncertain Variables

The first step in the methodology was to determine which parameters were uncertain and how they varied. Note that for purposes of this project, the values and distributions used needed to be representative, but not extremely accurate, as the application of the method was the goal, and not the actual results.

In the fluid component of the simulations, the uncertain variables included the density of air, the angle of attack of the wing, and the air speed of the plane. For our model, it was assumed that the aircraft was flying at an altitude of 9,000 meters, which is safely below the ceiling cruising altitude of the trainer. Even though flight profile was at a constant altitude, the density of air could still have some variability. At an altitude of 9,000 meters, the nominal density of air is 0.4671 kilograms per cubic meter [27]. A five percent deviation was used with a normal distribution to form the probability distribution for the air density input. This distribution was chosen because at Mach 0.3 there is a five percent variation in the ratio of the density of the fluid in motion to the density of the fluid at rest [27].

Transient flight conditions result in a variety of dynamic loads and conditions. In order to use the vortex lattice method as a surrogate fluid dynamics model as described below, the angle of attack needed to be small and not near the stall angle of attack since the method uses the small angle approximation and does not account for the onset of a stall. Taking these factors into account, we simulated the plane at a nominal angle of attack of eight degrees with a variability of plus or minus two degrees with a uniform distribution.

In order to account for variation of bulk air movement during flight, the air speed was also considered to be an uncertain variable. Air speed is the relative speed of the air flowing by the plane. As the wind changes mid flight, so does the relative air speed. In order for the vortex lattice method to be valid, the flow field must be incompressible. For incompressibility, the air speed should not be over Mach 0.3. Thus, the nominal air speed was set at 91.2 meters per second, which corresponds to Mach 0.3 at an altitude of 9000 meters. A uniform distribution with a plus and minus five meters per second was used for the variation in airspeed.

The structural surrogate model had its own set of uncertain variables. Two of these variables, Young's modulus and Poisson's ratio, are material properties of the 7075-T6 aluminum of which most of the wing is constructed. The Young's modulus for 7075-T6 is 10,400 ksi, and Poisson's ratio is 0.33. Not every sheet of aluminum has the exact same mechanical properties; there are slight differences in the heat treatment or the alloy composition of two different sheets of metal. In order to capture this variability, both the Young's modulus and Poisson's ratio were assigned a variability of plus or minus five percent.

The final two uncertain variables considered in the structural model were the yield strength and the ultimate tensile stress for 7075-T6 aluminum. There is a range of acceptable values for these properties, with the lower limit set by the lowest permissible yield and ultimate strengths according to US standards. The lowest acceptable value for the yield strength of 7075-T6 aluminum is 62 ksi [28]. However, this value is typically as high as 73 ksi [29]. The 7075-T6 aluminum must have an ultimate tensile strength of at least 71 ksi [28], but it can be as much as 83 ksi [29]. Table 1 summarizes the uncertain parameters for the simulations. In the next section the technique used for sampling from these variable distributions is discussed.

Table 1. Data on Fluid and Structure Parameters

PARAMETER	SYMBOL	NOMINAL	UNITS	DISTRIBUTION	VARIABILITY
Air density	ρ_{air}	0.4671	kg/m^3	Normal	5%
Angle of attack	α	8	degrees	Uniform	25%
Air speed	-	91.2	m/s	Uniform	5.48%
Young's modulus	E	10400	ksi	Normal	5%
Poisson's ratio	v	0.33	-	Normal	5%
Yield strength	σ_y	67.5	ksi	Normal	7.41%
Ultimate strength	σ_{uts}	77	ksi	Normal	7.79%

2.2.3.5 Latin Hypercube Sampling

The probability distributions used to represent the uncertainties in the fluids and structural components need to be propagated through the computational models in order to obtain the variation of the dependent variables or system response quantities (SRQs) of the models. Since the uncertainties in the independent variables were modeled using probability distributions, probability theory was used to propagate the uncertainties to the dependent variables.

Often, Monte Carlo sampling is used, in which random samples are taken from the probability distribution of each input. Nominal Monte Carlo requires many samples to be taken in order to adequately characterize the input probability distributions. One computer run must be done for each random sample. In order to characterize the entire set of distributions, thousands of samples need to be formed, which in turn requires thousands of computer runs. This process is inefficient, especially if the tails of the distribution are the real interest, and for long-running simulation codes, is actually impossible in many cases.

A form of Monte Carlo sampling, known has Latin Hypercube Sampling (LHS), is a popular choice of experimental design when computer simulation is used to study a physical process. LHS designs guarantee uniform samples for the marginal distribution of each single input. When sampling a function of N variables, the range of each variable is divided into M equally probable intervals. M sample points are then placed to satisfy the Latin hypercube requirements; note that this forces the number of divisions, M, to be equal for each variable. Also note that this sampling scheme does not require more samples for more dimensions (variables); this independence is one of the main advantages of this sampling scheme. Another advantage is that random samples can be taken one at a time, remembering which samples were taken so far.

The LHS process was applied to the seven input parameters and their probability distributions as described in Table 1. Since we want an accurate characterization of the outputs, 500 samples were used, although this number was arbitrary and could have been larger or smaller. This means that for each input parameter there were five samples for each percentile of the distribution, which ensured that the tails of the distributions were well characterized to approximately the 0.002 probability level. Each sample set has one sample member from each parameter. The 500 sets formed a matrix, which will be referred to as the LHS sample matrix.
Using a conventional approach, 500 simulations of *Rocflo* and *Abaqus* would have been needed, which is impractical. However, reducing the number of sample sets to a number that creates a plausible number of simulation runs on *Rocstar* (e.g., five to ten) would severely limit the accuracy of the final output distributions. The solution proposed to this problem of computational limits is to use a low-order surrogate physics model coupled with a clustering methodology.

2.2.3.6 Clustering Methodology Overview

The clustering methodology was proposed at a Sandia National Laboratories Validation Workshop [30], and was initially applied for uncertainty analysis on CFD in solid propellant rockets [31]. Large sample sets were used to maintain the details of the input distributions. Only a few high-fidelity multi-physics simulations are assumed possible due to resource constraints.

Also, it is assumed that some of the LHS sample sets will produce results similar to one another, and that one sample from a group of samples that produce similar results can be selected to represent the aggregate group. In order to identify the representative sample set, low-order surrogate models are used to predict the approximate response of the SRQs. These predictions are then organized into clusters, in which each cluster groups the predictions that have similar results. A representative sample is chosen from each cluster and is used for large scale multi-physics simulations. The results from the full scale simulations are interpolated with the results from the surrogate models to create the output distribution. This is a brief overview of the methodology and each aspect of the methodology is examined in more detail as it applies to the demonstration in the following sections.

2.2.3.7 Surrogate Models

One of the important aspects of the methodology is the selection of the low-order surrogate models. Surrogate models are analytical equations or fast running computer simulations that *quickly* predict the SRQs. The surrogate models are used to predict the response of a SRQ for each element in the LHS matrix. Then the results produced by the surrogate models are clustered as describe in section 2.2.3.6, and a representative sample set of input values is chosen for each cluster. The main purpose of the surrogate model is to define the shapes of the SRQ distributions in relation to the input probability distributions. The surrogate models capture the trends, not the exact values, of the output parameter correctly. The models chosen should give similar result trends to those that would be seen if the *Rocstar/Abaqus* models were run for each LHS sample member. A few full-scale detail simulations are then performed to allow interpolating the surrogate results into a more "accurate" space.

Since these simulations contain a fluid and structure component, surrogate models were developed that captured the uncertainty trends in both. The main focus of the project was predicting the structural response rather than the fluid response; consequently, several structural surrogate models of differing degrees of fidelity were tested to investigate the impact of the surrogate models on the output parameter's probability distribution.

2.2.3.7.1 Fluids Surrogate Model

For the fluids component of the problem, the surrogate model involved the three uncertain variables: the angle of attack, air density, and the airspeed. These variables were propagated into the model in the form of lift on the wing. The total lift on an airplane can be found using Equation 1:

$$Lift = \frac{1}{2} C_L \rho_{air} U_\infty^2 S \tag{16}$$

where C_L is the lift coefficient, ρ_{air} is the air density, and U_∞ is the freestream air velocity. The angle of attack is incorporated into the lift coefficient, and thus is also a variable of the total lift. S represents the planform area of the wing; however this was not an uncertain variable since the geometry of the plane was assumed constant within tolerances that will not affect the aerodynamics of the aircraft.

The lift coefficient and thus the total lift were calculated using the Matlab program *Tornado* [32]. This program uses the vortex lattice method to describe the airflow around the wing of an aircraft. A few assumptions need to be made about the flow field in order for this method to be valid. The flow field must be incompressible and irrotational. Also, viscous forces are ignored and the angle of attack must be small, so that the small angle approximation may be used.

In *Tornado*, the geometry of the wing of the trainer had to be approximated. Inputs included the root chord length, the dihedral and sweep of the wing, the taper ratio, and span of the wing. In order to create the correct airfoil, coordinates of the NACA 65A004.8 airfoil were normalized and then imported into *Tornado*. The geometry and airfoil of the trainer represent constant properties that do not contain uncertain variables. The uncertain variables appeared in the description of the state, or environment, of the aircraft.

The fluid uncertainty variables were propagated through *Tornado* and the total lift was recorded. The total lift was used in the structural surrogate models to determine the magnitude of the lift distribution.

2.2.3.7.2 Structural Surrogate Models

Each of the structural surrogate models was created using the same basic assumptions. The wing was considered to be entirely made from Al 7075-T6. Next, the wing was assumed to be under an elliptical lift distribution, as described in Equation 2, where L is the length of the wing and x is the distance along the wing measured from the wing root. The variable f_0 refers to the magnitude and is calculated in Equation 3.

$$F(x) = f_0\left(1-\frac{x^2}{L^2}\right) \tag{17}$$

$$f_0 = \left(\frac{3}{4L}\right)*(Lift) \tag{18}$$

It was assumed that the wing was under pure bending, i.e., the wing to behaved like a beam. The wing was approximated as a cantilever beam since the dimensions of its airfoil were small compared to the longitudinal axis of the wing. Although the cross section of the wing does not change in shape, there is a gradual decrease in size. Because of this, the moment of inertia was averaged in order to make it constant and simplify the calculations. This average inertia was taken at the Mean Aerodynamic Chord (MAC). The MAC is the characteristic chord at which the average properties of the airfoil can be determined. When the airfoil at this chord was modeled in *Abaqus*, a moment of inertia of 16719.3 in^4 was calculated. This value was assumed to be the average inertia of the airfoil across the entire wing. The cross section contained an effective skin thickness that incorporated the top and bottom flanges of seven main spars. Drag was ignored and the twisting of the wing due to the shear stress was not modeled.

2.2.3.7.3 Castigliano's Theorem Model

The first structural surrogate model uses Castigliano's theorem, i.e., the derivative of the total strain energy of an elastic system with respect to the force acting at a specific location is equal to the displacement at that location.

$$U = \frac{1}{2}\int_0^L \frac{M_z^2}{EI}\,dx \tag{19}$$

$$\frac{\partial U}{\partial Q_i} = q_i \tag{20}$$

Equation 4 shows how the strain energy (U) for the idealized wing is calculated. In order to simplify this analysis, it was assumed that Young's modulus, E, and the moment of inertia, I, of the airfoil were both constants for any single realization of the model. To find the moment associated with the wing, M_z, it was assumed that an elliptic lift curve was distributed over the entire span of the wing. In Equation 5 the term q_i refers to the displacement at a specific point of the beam, while Q_i is the generalized force at that point. Since we were interested in the displacement at the wing tip, a "dummy load" (P_D) was required at the wing tip. In order to account for this dummy load, Equation 5 was adjusted:

$$w(L) = \lim_{P_D \to 0}\left(\frac{\partial U}{\partial P_D}\right) \tag{21}$$

where w(L) is the displacement of the wing tip in the z direction. Each sample member in the LHS sample was processed with this model (using the fluids surrogate model from section 2.2.3.7.1 to produce the load), and an estimate of the wing tip displacement was generated for each sample.

2.2.3.7.4 Euler-Bernoulli Beam Model

Euler-Bernoulli beam theory was the second surrogate model. Equation 7 shows the wingtip displacement, where f_0 is the load factor, L is the length of the wing or half the span, E is Young's modulus, and I is the second area moment of inertia.

$$w(L) = \frac{19 f_0 L^4}{360 EI} \tag{22}$$

The load factor, f_0, was determined by the total lift which was calculated using the fluid surrogate model. The uncertainty is propagated through Young's modulus and the load factor. The surrogate model was run 500 times with the LHS matrix and the displacement recorded.

2.2.3.7.5 Abaqus Beam Model

The *Abaqus* wing-beam model used the Meshed Beam Cross-Section (MBCS) approach described in the *Abaqus* documentation [33]. MBCS allows structures with complex geometry, which exhibit characteristics of beams, to be modeled without having to create a 3D model. It is a two-step process in which the cross sectional properties are calculated separately, in meshed cross section models, and then assigned to the corresponding segments of the beam model for the beam analysis. This surrogate model had the highest degree of fidelity of the three solid mechanics surrogates because it accounted for varying geometry.

In order to model the swept and tapered wing, the wing was partitioned into five segments that were separated by ribs. Each segment had a constant cross section that was defined by the cross section of the MAC for that segment. This resulted in decreasing cross sections that modeled the geometry of the wing. Each cross section modeled the skin and spars as one piece. MBCS does not model the contact or riveting between structural components. The skin-spar part was modeled using warp elements and assumed linear isotropic elastic material. This material captured the uncertain parameters of Young's modulus and Poisson's ratio. From the cross section models, an out-of-plane warping function and the cross section properties were calculated (area moment of inertia, torsion constant, shear center, etc.). These were utilized in the beam analysis.

Using MBCS, the wing was modeled as a cantilever beam with linear beam elements. These elements used Timoshenko beam theory. The cross sectional properties that were defined in the meshed cross section models were assigned to the linear beam elements that represent that segment of the wing. In *Abaqus*, a pressure distribution cannot be applied to linear beam elements; consequently, for each segment a force resultant was applied. The beam analysis was conducted and the wing tip displacement found for each of the LHS sample members.

2.2.3.8 Clustering

Restrictions on the number of computer simulations that can be performed occur frequently. In our case, the time needed to run the fluid flow solver, *Rocflo*, was the main restriction to the number of simulations that could be performed. We did not have time to run 500 separate *Rocflo* simulations, so we limited the number of full scale runs to six. To select the six LHS sets, the LHS matrix was processed with the fluid surrogate model. The resulting wing loads were then used in each structural surrogate model and the wing tip displacements found for each sample member in the LHS matrix. In this methodology, the number of clusters required is one less than the total number of high-fidelity *Rocstar/Abaqus* simulations that are planned.

Using the wing tip displacements, The 500 displacements for each surrogate model were clustered into five groups. Each cluster represents a set of samples that predicted similar displacements of the wing tip. This clustering process was done using SPSS, a statistical package that employs a K-means clustering algorithm. This type of algorithm is a partitional method where the number of clusters must be predefined by the user. The clusters for the Castigliano's Theorem, the Euler-Bernoulli Beam Theorem, and the *Abaqus* Beam surrogates are

shown in Figures 7 to 9. Each circle on the graph represents the wing tip displacement of one of the members of the LHS matrix.

The representative samples that were to be run in the full scale multi-physics simulations were selected based on these clusters. There are different ways in which this could be done [34]. The effects of the extreme values are of importance since the goal was to create probability distributions for various properties of the wing. The best way to capture the extreme values is to take the first and last sample member of each cluster after they are sorted in ascending order by the wing tip distribution. Using this method, a total of ten sets of input parameters were collected from the five clusters.

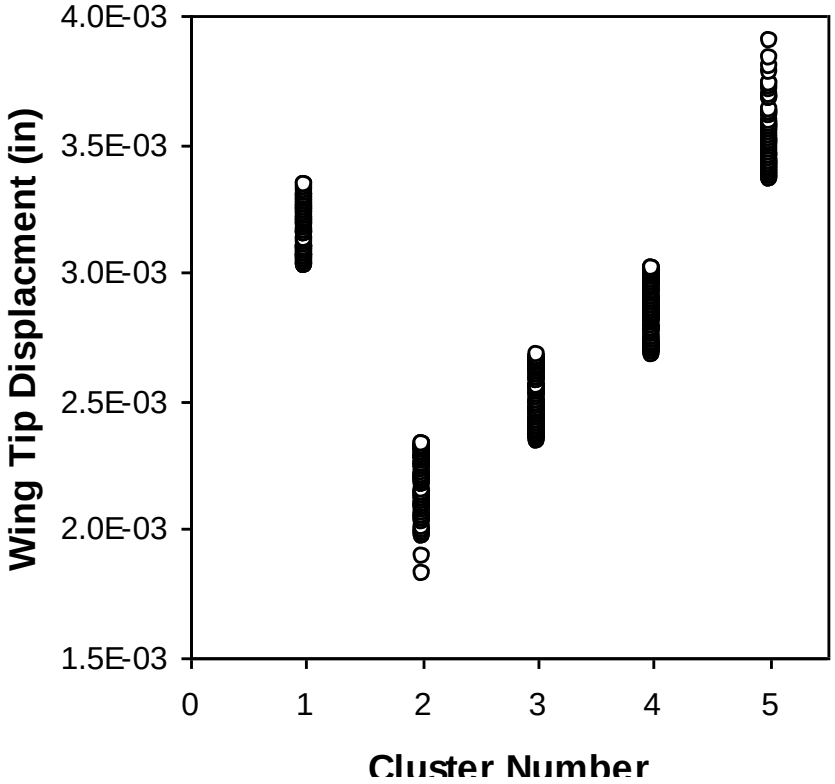

Figure 7: Cluster ranges for Castigliano's Theorem model

However, the lowest sample of a cluster and the highest sample of a previous cluster have almost identical responses since the range of wing tip displacements was almost continuous, as seen in Figures 6 to 8. Since the *Rocstar* responses should be similar, it is only necessary to take one of the two values from each cluster interface. Thus, by taking only the sample member with the highest displacement for each cluster and also the lowest sample in the lowest cluster, the number of simulations was reduced to six.

The CFD parameters from the six selected sample members were used in six *Rocflo* runs. Each of those *Rocflo* runs was performed with its unique set of parameters, and the pressures that developed on the surfaces of the wing during the simulation were extracted and then applied to

an *Abaqus* model using the corresponding Solid Mechanics parameters for the given sample. The *Abaqus* model was then run, and a wing tip displacement was found. This provides "high-fidelity" estimates of the wing-tip displacement for six cases. These six high-fidelity results were then mapped onto the distribution estimated from the surrogate model results. This is achieved by interpolating between the high-fidelity results based on the surrogate-model results. This effectively "pinned" the SRQ distribution at six points (including the extrema) based on the high-fidelity results, and then the shape of the distribution between those points was based on the low-order surrogate results. Thus, the accuracy of the surrogate models is not important; they just need to predict the trends correctly.

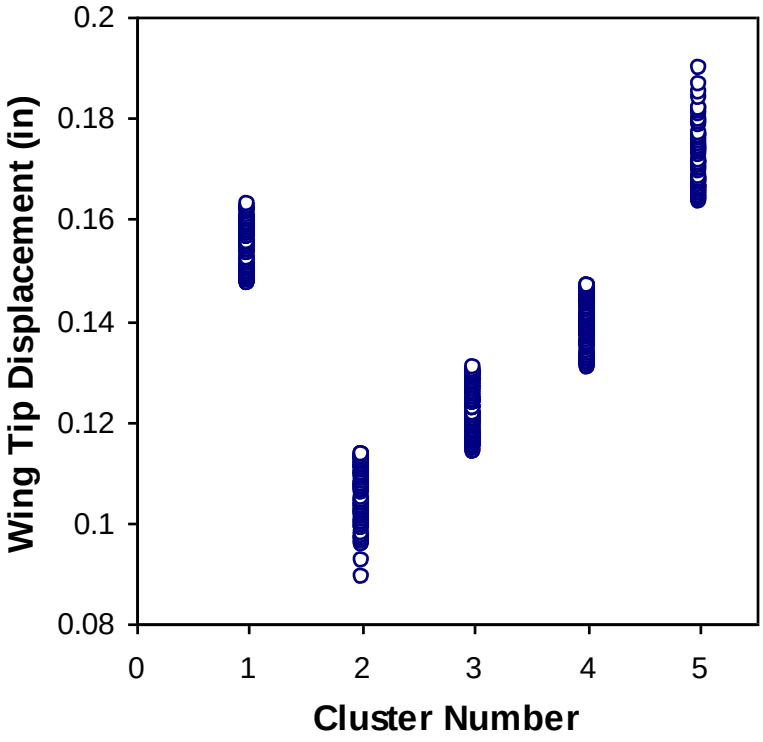

Figure 8: Cluster ranges for Euler-Bernoulli model

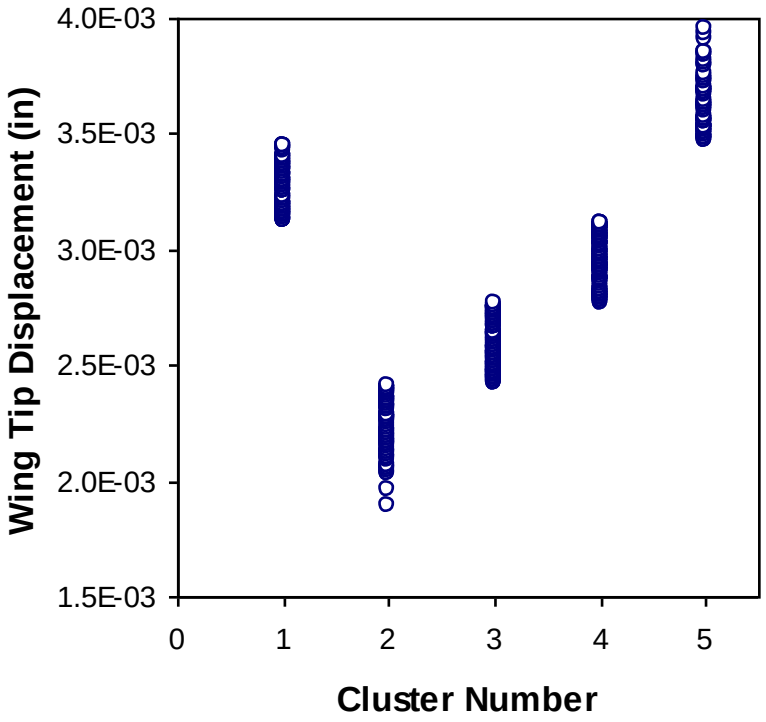

Figure 9: Cluster ranges for the *Abaqus* beam model

2.2.3.9 Results

One of the goals of this project was to investigate the effects that different surrogate models would have on the final output probability distributions. The trends of the output distributions are most impacted by the surrogate models. In Figure 9, the normalized wing tip displacements for each surrogate model are shown for each sample set in the LHS matrix. The results trends are almost exactly the same. This is to be expected because Castigliano's Theorem and the Euler-Bernoulli surrogate models are different methods to reach the same conclusion. The *Abaqus* beam model provided more accurate values for the displacement; however, because the analysis was linear, it provided a very similar trend to the other models.

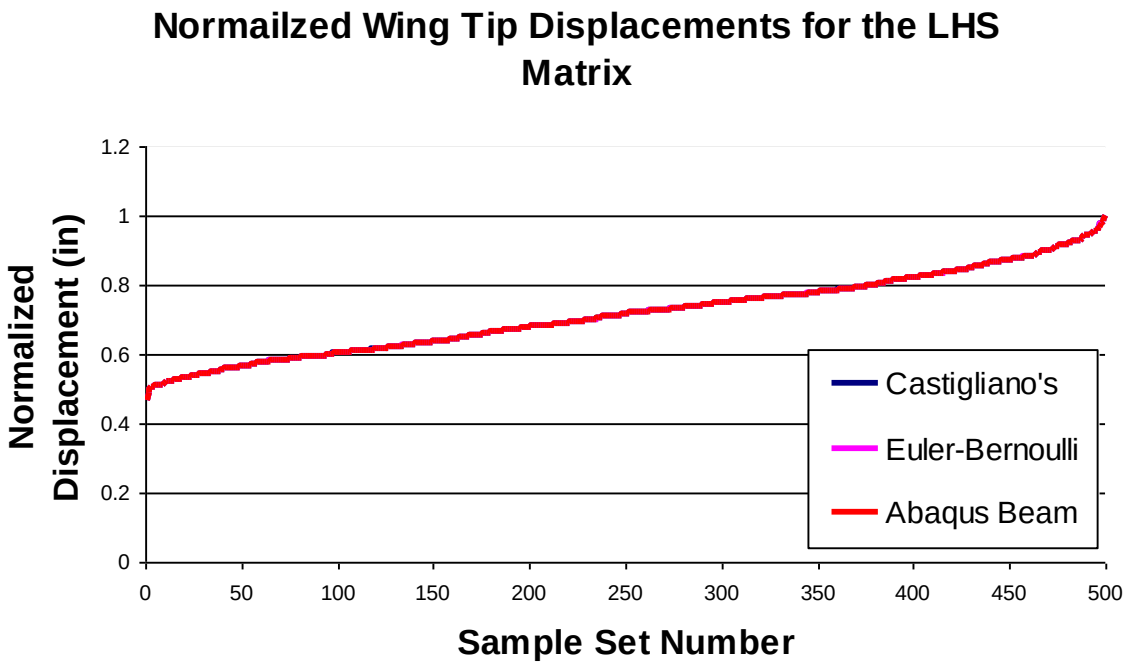

Figure 10: The normalized displacements comparing trends of the surrogate models

The final step in the uncertainty assembly has been attempted using this methodology. The results, however, were disappointing from the perspective that the displacements calculated in *Abaqus* based on the transferred CFD pressures were very small. This may be due to limited runtime for the CFD simulations, the limited angle of attack able to be simulated due to the surrogate model limitations, or errors in the pressure transfer algorithms that were developed for this work. The direction of this project was redirected before it was possible to ascertain where the problem exists. Thus, while the overall process appears to be feasible in a Fluid-Structure-interaction problem, a complete end-to-end assessment will be a future project.

3.0 CONCLUSIONS AND RECOMMENDATIONS

Probabilistic methods applied to ensuring structural integrity show promise as they have for the past 30 years. The challenge does not seem to be in developing new more sophisticated probabilistic techniques, but in getting the techniques into common practice. It needs to become relatively easy for the average engineer without a lot of expertise to use probabilistic methods. The way to do this is to make incremental changes to existing design and maintenance processes by enabling engineers to readily obtain more and better information upon which to base any decisions about the airworthiness of an aircraft upon. This should be the focus of future efforts on Risk-Quantified Structural Design and Evaluation.

4.0 References

1. Tuegel, E., Olson, S.E., and Braisted, W.R., "Risk Quantified Structural Design and Evaluation," AFRL-VA-WP-TR-2007-3040 (ADA469891), May 2007.
2. Tuegel, E., Olson, S.E., Braisted, W.R., and Frank, G.J., "Risk-Quantified Thermal Buckling Analysis," AFRL-VA-WP-TR-2007-3039, April 2007.
3. Southwest Research Institute, "NESSUS Overview", www.nessus.swri.org/, 2009.
4. Prediction Probe, Inc., "UNIPASS™", www.predictionprobe.com/prod_unipass.htm, 2008.
5. Smith, L., Millwater, H., Griffin, K., and Wieland, D., "Advanced Structural Reliability Methods for Aircraft Structures," 49th AIAA/ASME/ASCE/AHS/ASC Structures, Structural Dynamics and Materials Conference, 7-10 April 2008, Schaumburg, IL, AIAA 2008-
6. Domyancic, L., Sparkman, D., Millwater, H., Smith, L., and Wieland, D., "A Fast First Order Method for Filtering Limit States," 50th AIAA/ASME/ASCE/AHS/ASC Structures, Structural Dynamics and Materials Conference, 4-7 May 2009, Palm Springs, CA, AIAA 2009-2260.
7. Penmetsa, R., Kable, B., and Tuegel, E., "Identifying Structurally Significant Items Using Matrix Re-analysis Techniques," 50th AIAA/ASME/ASCE/AHS/ASC Structures, Structural Dynamics and Materials Conference, 4-7 May 2009, Palm Springs, CA, AIAA 2009-2259.
8. Pinto, J.T., Blockley, D.I., and Woodman, N.J., "The Risk of Vulnerable Failure," *Structural Safety*, 24, pp. 107-122, 2002.
9. Tuegel, E., and Penmetsa, R., "Risk-Based Design and Certification of Aircraft: A Systems Engineering Approach," 47th AIAA/ASME/ASCE/AHS/ASC Structures, Structural Dynamics and Materials Conference, 1-4 May 2006, Newport, RI, AIAA 2006-2147.
10. Penmetsa, R., and Tuegel, E., "Risk Quantified Static Strength Design of Aircraft Structural Components," 48th AIAA/ASME/ASCE/AHS/ASC Structures, Structural Dynamics and Materials Conference, 23-26 April 2007, Honolulu, HI, AIAA 2007-1970.
11. Dwire, H., Penmetsa, R., and Tuegel, E., "Risk-Based Design Plots for Aircraft Damage Tolerant Design," 49th AIAA/ASME/ASCE/AHS/ASC Structures, Structural Dynamics and Materials Conference, 7-10 April 2008, Schaumburg, IL, AIAA 2008-2077.
12. Tuegel, E., Penmetsa, R., and Shanmugam, V., "Probability of Fracture Nomographs for Quick Risk Assessment," 2008 Aircraft Structural Integrity Program Conference, 2-4 Dec 2008, San Antonio, TX.
13. Tuegel, E., Penmetsa, R., and Shanmugam, V., "Rapidly Assessing the Probability of Fracture for Stiffened Panels," 12th International Conference on Fracture, 13-16 July 2009, Ottawa, Ontario.
14. Basu, A. P., and Lochner, R. H., "On the Distribution of the Ratio of Two Random Variables Having Generalized Life Distributions," *Technometrics*, Vol. 13, pp. 281–287, 1971.
15. Bhargava, R. P., and Khatri, C. G., "The Distribution of Product of Independent Beta Random Variables With Application to Multivariate Analysis," *Annals of the Institute of Statistical Mathematics*, Vol. 33, pp. 287–296, 1981.
16. Hawkins, D. L. and Han, C. P., "Bivariate Distributions of Some Ratios of Independent Noncentral Chi-square Random Variables," *Communications in Statistics --Theory and Methods*, Vol. 15, pp. 261–277, 1986.
17. Korhonen, P. J., and Narula, S. C., "The Probability Distribution of the Ratio of the Absolute Values of Two Normal Variables," *Journal of Statistical Computation and Simulation*, Vol. 33, pp. 173–182 1989.
18. Malik, H. J., and Trudel, R., "Probability Density Function of the Product and Quotient of

two Correlated Exponential Random Variables," *Canadian Mathematical Bulletin,* Vol. 29, pp. 413– 418, 1986.
19. Marsaglia, G., "Ratios of Normal Variables and Ratios of Sums of Uniform Variables," *Journal of the American Statistical Association,* Vol. 60, pp. 193–204, 1965.
20. Nadarajah, S., and Gupta, A. K., "Products of Random Variables with Cauchy Kernel," *Pan American Journal of Mathematics,* Vol. 15, pp. 47–56, 2005.
21. Pham-Gia, T., "Distributions of the Ratios of Independent Beta Variables and Applications," *Communications in Statistics --Theory and Methods,* Vol. 29, pp. 2693–2715, 2000.
22. Nadarajah, S., and Kotz, S., "On the Product and Ratio of Gamma and Weibull Random Variables," Econometric Theory, Vol. 22, pp. 338-344, 2006.
23. Podolski, H., "The Distribution of a Product of *n* Independent Random Variables with Generalized Gamma Distribution," *Demonstratio Mathematica,* Vol. 4, pp. 119–123, 1972.
24. Penmetsa R. C., and Grandhi R. V., "Adaptation of Fast Fourier Transformations to Estimate Structural Failure Probability," Journal of Finite Elements in Analysis and Design, Vol.39, No. 5-6, pp. 473-486, 2003.
25. Benjamin, J. R., and Cornell, C. A., Probability, Statistics and Decision for Civil Engineers, McGraw-Hill, New York, 1970.
26. Glen, A. G., Leemis, L. M., and Drew, J. H., "Computing the Distribution of the Product of Two Continuous Random Variables," Computational Statistics and Data Analysis, Vol. 44, pp. 451-464, 2004.
27. Anderson, John D., Jr., *Fundamentals of Aerodynamics*, 4th Edition, McGraw-Hill, Boston, 2007, pp. 534-535, 966.
28. Cutler, John, *Understanding Aircraft Structures*, 4th Edition, Blackwell Publishing, Malden, MA, 2005, pp. 90-91.
29. Callister Jr., William D., *Fundamentals of Materials Science and Engineering: An Integrated Approach*, 2nd Edition, John Wiley & Sons, Inc., Danvers, MA, 2006, pp. A12.
30. Brandyberry, M. D., "Thermal Problem Solution Using a Surrogate Model Clustering Technique," *Computer Methods in Applied Mechanics and Engineering*, Vol. 197(29-32), pp. 2390-2407, 2008.
31. Brandyberry, M. D., *Uncertainty Quantification in 3D Rocket Simulation,* AIAA-2006-4586, presented at the American Institute of Aeronautics and Astronautics JPC meeting, July 2006.
32. Melin, Tomas, "Tornado: The Vortex Lattice Method," Royal Institute of Technology/University of Bristol, Stockholm/Bristol, December 18, 2007, [http://www.redhammer.se/tornado/index.html. Accessed 6/27/2008.]
33. *Abaqus Analysis User's Manual,* Volume II, Version 6.8, ABAQUS, Inc., 2008, pp. 10.5.1-1.
34. Brandyberry, M., and E. Egejuru, "Uncertainty Quantification for Multiphysics Solid Rocket Motor Simulations," 54th Joint Army-Navy-NASA-Air Force (JANNAF) Propulsion Meeting (JPM), May 14-17, 2007, Denver, CO.